Magnetic and structural phase transitions in erbium at low temperatures and high pressures

Sarah A. Thomas, Georgiy M. Tsoi, Lowell E. Wenger, Yogesh K. Vohra, and Samuel T. Weir

Phys. Rev. B **84**, 144415 — Published 10 October 2011

DOI: 10.1103/PhysRevB.84.144415

Magnetic and Structural Phase Transitions in Erbium at Low Temperatures and High Pressures

Sarah A. Thomas, Georgiy M. Tsoi, Lowell E. Wenger, and Yogesh K. Vohra

Department of Physics, The University of Alabama at Birmingham (UAB)

Birmingham, AL 35294, USA

and

Samuel T. Weir

Mail Stop L-041, Lawrence Livermore National Laboratory (LLNL)

Livermore, CA 94550, USA

Electrical resistance and crystal structure measurements have been carried out on polycrystalline erbium (Er) at temperatures down to 10 K and pressures up to 20 GPa. An abrupt change in the slope of the resistance is observed with decreasing temperature below 84 K which is associated with the *c*-axis modulated antiferromagnetic (AFM) ordering of the Er moments. With increasing pressure, the temperature of the resistance slope change and the corresponding AFM ordering temperature decrease until vanishing above 10.6 GPa. The disappearance of the slope change in the resistance occurs at similar pressures where the hcp structural phase of Er is transformed to a nine-layer α-Sm structural phase as confirmed by our high-pressure synchrotron X-ray diffraction studies. These results suggest that the disappearance in the antiferromagnetic ordering of Er moments is strongly correlated to the structural phase transition at high pressures and low temperatures.

PACS: 62.50.-p, 74.62.Fj, 64.70.K-

I. INTRODUCTION

The heavy rare earth metal erbium, Er, has been the subject of numerous investigations to study the magnetic transitions and accompanying magnetic structures as a function of temperature at ambient pressure. Three distinct magnetic phase transitions have been reported [1-6]: (i) a *c*-axis modulated (CAM) antiferromagnetic (AFM) structure below 84 K, in which the Er magnetic moments are sinusoidally ordered with the modulation vector aligned along the *c*-axis, (ii) a nearly planar elliptical cycloidal structure below 52 K with the moments aligned in the *a*-*c* plane, and lastly (iii) a ferromagnetic conical structure at 18 K in which the ferromagnetic component lies along the *c*-axis. These magnetic transitions are also manifested by temperature-dependent changes in the electrical resistivity [7,8], magnetization [8,9], heat capacity [10,11], and magnetostriction [12-14]. While these temperature-dependent changes are most dramatic in single crystalline samples in which measurements and applied magnetic fields are along a specific crystallographic axis of the hexagonal-close-packed (hcp) structure of Er, the transitions to the CAM antiferromagnetic and ferromagnetic conical structures are typically observable in measurements on polycrystalline samples as well. For example, the electrical resistivity along the *c*-axis of an Er single crystal [8] exhibits an abrupt increase at the antiferromagnetic Néel transition temperature T_N with decreasing temperature, followed by a sharp decrease in resistivity at the temperature of the elliptical cycloidal transition T_{CY}, and then a small discontinuous drop in resistivity at the ferromagnetic temperature T_C. On the other hand, the resistivity along the *a*-axis only exhibits changes in slope at each of these transition temperatures. In comparison, the electrical resistivity on polycrystalline Er samples [7] at ambient pressure just displays a small, but discernible, change in slope at T_N.

Studies of the magnetic properties and magnetic structures of Er under pressure are more limited, especially at pressures in the GPa range. Neutron diffraction studies of the magnetic structure by Kawano, *et al.* [15,16] found at 1.15 and 1.4 GPa pressure that the transition to the ferromagnetic conical structure is completely suppressed with the elliptical cycloidal structure persisting down to 4.5 K. The CAM antiferromagnetic ordering decreased from 84 K at ambient pressure to 82 K at 1.4 GPa pressure while the cycloidal structure at 1.4 GPa was initially observable at 46 K. The suppression of the low-temperature ferromagnetic conical structure under pressure was confirmed by another neutron diffraction study [17] at 6.0 K which suggested at pressures as low

as 0.5 GPa that the conical phase is destroyed. Other studies of the pressure-vs.-temperature phase diagrams are based on a very limited number of pressure-dependent resistivity and magnetic susceptibility measurements. Milton and Scott [18] found from magnetic inductance measurements up to 0.7 GPa that the antiferromagnetic transition decreased with pressure from 85 K as dT_N/dP = -2.6 ± 0.1 K/GPa. Ellerby, *et al.* [19] developed a more detailed *p-T* diagram from resistivity measurements on single-crystal erbium in the pressure range from 0 to 1.2 GPa and found similar values for the Néel temperature and its pressure dependence, 85.5 ± 0.1 K and -3.1 ± 0.2 K/GPa, respectively. More recently Jackson, *et al.* [20] carried out ac magnetic susceptibility measurements on a series of heavy rare earth metals to 21 GPa and observed that magnetic signals disappeared at varying high pressures including the disappearance of the magnetic signal at the AFM transition in Er around 11 GPa with a dT_N/dP = -3.1 ± 0.2 K/GPa. However, the reason for this disappearance was not well understood due to a lack of structural data at high pressures and some uncertainty as to whether the disappearance was the result of the experimental resolution of the measurements. In this report, we have addressed this critical issue by performing structural measurements at low temperatures and high pressures in combination with pressure-dependent electrical resistance measurements in order to correlate the structural transitions to magnetic phase transitions.

II. EXPERIMENTAL

High-pressure electrical resistance and X-ray diffraction measurements were carried out using diamond anvil cells at pressures up to 20 GPa on pieces cut from a 0.1-mm thick foil of polycrystalline Er [21]. The X-ray diffraction pattern observed on the Er foil at ambient pressure indicated a textured structure with a *c*-axis preferred orientation normal to the foil surface. This *c*-axis preferred orientation was also observable in the temperature dependence of the magnetic susceptibility [22] on Er disks cut from the foil as shown in Fig. 1. The CAM antiferromagnetic transition at 82 K is easily discernible for fields normal to the disk surface while the AFM transition is only detectable at higher magnification for magnetic measurements parallel to the disk. Electrical resistance measurements under pressure were performed using eight-probe designer diamond anvils [23,24] in a four-probe configuration on pieces cut from the foil and loaded along with a ruby pressure sensor into an 80-micron diameter sample chamber. The eight tungsten microprobes are encapsulated in a homoepitaxial diamond film and are exposed only

near the tip of the diamond to make contact with the erbium sample at high pressure. Two electrical leads are used to set constant dc current through the sample and two additional leads are used to monitor the voltage across the sample. The pressure was monitored by the ruby fluorescence technique and care was taken to carefully calibrate the ruby R_1 emission at low temperatures as described in an earlier publication [25]. Two separate electrical resistance experiments with different Er pieces were carried out to check the reproducibility of the magnetic transitions observed at various pressures. In addition, some data points were obtained during decompression to establish the reversibility of magnetic phase transition. The high-pressure X-ray diffraction experiments on polycrystalline Er were carried out at the beam-line 16-BM-D, HPCAT, Advanced Photon Source at Argonne National Laboratory to low temperatures using a diamond anvil cell. An angle-dispersive technique with an image-plate area detector was employed using an X-ray wavelength λ = 0.4134 Å. The pressure was determined from the diffraction peaks of copper which was also loaded into the diamond anvil cell with Er and using the Birch-Murnaghan equation [26] of Eq. 1 with the available equation of state data for the copper pressure standard [27],

$$P = 3B_0 f_E (1+2f_E)^{5/2}\left\{1+\frac{3}{2}(B'-4)f_E\right\} \qquad (1)$$

where B_o is the bulk modulus, B' is the first derivative of bulk modulus at ambient pressure, and V_0 is the ambient pressure volume. The values for copper pressure standard are B_0 = 121.6 GPa, B' = 5.583, and V_0 = 11.802 Å^3/atom, and the parameter f_E is related to volume compression by:

$$f_E = \frac{\left[\left(\frac{V_o}{V}\right)^{2/3}-1\right]}{2} \qquad (2)$$

III. RESULTS

The measured electrical resistance results as a function of temperature for several pressures are displayed in Fig. 2a and 2b. All the data have been normalized to their 100-K resistance values so that the variation with pressures can be more easily discerned. Similar to ambient pressure

measurements on polycrystalline samples [7], the electrical resistance exhibits a linear temperature dependence for temperatures below 100 K followed by an abrupt change in slope of the electrical resistance around 84 K for the lowest pressure of 1.8 GPa. The temperature of this abrupt change in resistance slope shifts to lower temperatures as the pressure is increased until it disappears above a pressure of 10.6 GPa. At slightly higher pressures, the linear temperature dependence of the electrical resistance extends down to lower temperatures before a discernible downturn is observed around 40 K as shown in the 12.0 GPa data in Fig. 2b. At higher pressures, ~16 GPa and above, the resistance essentially exhibits a linear temperature dependence with no discernible slope change. As reported previously, the CAM antiferromagnetic transition is manifested experimentally by an abrupt change in the slope of the electrical resistance from its linear temperature dependence at T_N on polycrystalline Er samples at ambient pressure [7] as well on single crystal samples along the *c*-axis at pressures up to 1.2 GPa [19]. The precise location of this phase transition in the present electrical resistance data is facilitated by subtracting out the linear temperature dependent behaviour exhibited at the highest temperatures from the resistance data, and then drawing a line to the sloped and flat curves as shown in the inset in Fig. 3 where T_N is indicated for the resistance measurement at 1.8 GPa. Figure 3 shows the normalized resistance as a function of temperature for various pressures after a linear temperature dependent fit ($a+bT$) to the normalized resistance data between 80 K and 100 K has been subtracted. Clearly the change in slope of the resistance associated with the AFM transition is now seen as an abrupt "increase" which disappears above 10.6 GPa. At higher pressures, the resistance after the linear temperature dependence subtraction remains relatively temperature independent down to ~40 K and then displays a downturn which vanishes for pressures above 16 GPa. While some gradual variations in the resistance can still be observed in the highest pressure results in Fig. 3, these variations are within the experimental uncertainties of the measurements and therefore the overall electrical resistance for pressures above 16 GPa is essentially proportional to the temperature over the entire temperature range.

The overall temperature behaviour of the electrical resistance for the heavy rare earth metals including erbium [28,29] at ambient pressure has been generally attributed to (i) a temperature-independent contribution arising from residual impurity scattering, (ii) a contribution arising from phonon scattering that is given by the Grüneisen relation, which can be taken to be proportional to temperature except at the lowest temperatures, and (iii) a contribution due to spin

disorder scattering. The spin disorder contribution has been approximated as

$$\rho_s \propto \left[1 - \frac{\langle \mathbf{S} \rangle^2}{S(S+1)}\right] \qquad (3)$$

which correspondingly is proportional to the disorder of the magnetic moments. Thus above antiferromagnetic ordering temperature T_N, the spin disorder contribution would be a constant, independent of temperature, and would result in the overall temperature dependence of the total electrical resistance being linear, in agreement with our experimental results. At the onset of the antiferromagnetic transition, the resistance contribution due to the CAM antiferromagnetic spin order, i.e., $\langle \mathbf{S} \rangle^2 \neq 0$, would result in a decrease in the resistance from its linear temperature dependence. To explain the abrupt increase in the resistance at the onset of the CAM antiferromagnetic transition when measured along the *c*-axis for Er as well as at the magnetic ordering temperatures for other heavy rare earth metals, Macintosh [30] pointed out that the incommensurate periodic arrangement of the ordered magnetic moments along the *c*-axis gives rise to an extra periodicity in the electrostatic potential felt by the conduction electrons which introduces extra planes of energy discontinuity into the Brillouin zone structure normal to the *c*-axis. Correspondingly these additional Brillouin zone boundaries in the electronic structure of the rare earth metals result in additional scattering, so-called superzone scattering, and an increase in the resistance measured along the *c*-axis while having minimal effect on the resistance when measured in the basal plane [28-30]. For polycrystalline Er, the resistance would

be an admixture of the *c*-axis and basal plane resistances resulting in an abrupt change in resistance at T_N similar to the present experimental results. The observation of a downturn in the resistance around 40 K from the linear temperature dependence for pressures above 11 GPa once the CAM antiferromagnetic ordering has disappeared would still be the result of some other type of spin (magnetic) ordering assuming that the resistance contribution from the phonon scattering is still proportional to the temperature at these pressures. At the highest measured pressures, the absence of any discernible variations in the temperature dependence of the resistance would indicate the absence of any magnetic ordering at these pressures.

The pressure dependence of CAM antiferromagnetic Néel temperature T_N for two separate measurements (labeled run 1 and run 2) are in fairly good agreement with one another as shown in Fig. 4. In addition the T_N values determined from measurements during decompression (on decreasing pressure) from run 2 are also in reasonable agreement with values deduced from compression runs, indicating that that AFM phase was recovered on decreasing pressure. Since T_N appears to decrease with linearly with pressure up to 11 GPa, a least-squares-fit resulted in:

$$T_N \text{ (in Kelvin)} = 87 \pm 1 \; - \; 2.5 \pm 0.2 * P \text{ (in GPa)}$$

The slope dT_N/dP of – 2.5 K/GPa is in reasonable agreement with values of -2.6 and -3.1 K/GPa as reported from earlier high pressure magnetic inductance and resistivity experiments [18-20]. Since the magnetic ordering is thought to depend on competing interactions such as the RKKY exchange interactions, crystalline electric field effects, and anisotropic magneto-elastic effects [31], the application of a non-hydrostatic pressure along different crystalline directions as in this high-pressure resistance study on textured Er foil pieces might account for the difference in the values of dT_N/dP.

The disappearance of CAM antiferromagnetic transition in Er above 10.6 GPa as shown in Fig. 2 occurs at a similar pressure as previously reported from the most recent ac magnetic susceptibility measurements [20]. Since *f*-shell delocalization or a loss of magnetic moment are predicted to occur at pressures greater than 100 GPa in Er [32], X-ray diffraction measurements were undertaken at pressures up to 20 GPa at room temperature and in the 10 K to 100 K

temperature range in order to determine whether the disappearance of the AFM transition could be related to any structural or volumetric changes as observed on other rare earth metals [33]. At room temperature, the X-ray diffraction patterns indicate that Er is in the hexagonal-close-packed crystalline structure below about 8 GPa as evidenced by the (100), (101), (102), (110), (103), (200), and (201) diffraction peaks of the hcp phase as shown in Fig. 5a for measurements at 7.3 GPa. In comparison, the diffraction pattern at 11.2 GPa as shown in the upper pattern of Fig. 5 is significantly different with the peaks being indexed to the (011), (102), (014), (015), (110), (022) and (204) indices of the nine-layer hexagonal α-Sm structural phase. The diffraction pattern at 9.1 GPa (not shown) shows a mixture of both the hcp and α-Sm structural phases. Thus, the X-ray diffraction results at room temperature indicate that a structural shift from hcp to α-Sm is complete by a pressure of 11.2 GPa. High-pressure X-ray diffraction studies in the temperature range of 10 K to 100 K were also undertaken to verify that these structural phases persist at low temperatures. At lower temperatures, the temperature-dependent equation of state by Carter, *et al.* [34] was used with the available measured lattice parameters for copper pressure standard to determine the pressure. Similar to prior ambient pressure structural determinations [2,35,36], Er remains in the hexagonal-close-packed crystalline phase down to 10 K for pressures of 3.2 GPa and 4.6 GPa as shown in Fig. 5b. At 20.4 GPa, Er exists in the α-Sm phase down to 10 K as shown in the upper pattern of Fig. 5b. The corresponding lattice parameters for the hcp phase at 10 K are a = 3.504 Å and c = 5.390 Å at 3.2 GPa and a = 3.479 Å and c = 5.333 Å at 4.6 GPa, and those for the α-Sm phase at 10 K at 20.4 GPa are a = 3.192 Å and c = 21.955 Å. While these values of the a lattice parameters at 10 K for both structural phases are within the experimental uncertainty of the values determined at room temperature for similar pressures, the values of the c lattice parameters at 10 K for the hcp and α-Sm phases are approximately 1% and 5% smaller than their respective values at room temperature. Consequently, the observation of this structural change with no corresponding significant change in volume leads to the conclusion that the disappearance of the AFM transition as observed in the resistance measurements arises from a structural change from hcp to α-Sm rather than a volumetric change. Furthermore, this disappearance of the CAM antiferromagnetic transition in Er with the structural change from hcp to α-Sm can be explained in terms of the indirect exchange coupling between the Er moments via the conduction electrons being significantly different for the two structural phases. Nesting regions on the Fermi surface of rare earth metals are believed to give

rise to a peak in the conduction-electron susceptibility at a non-zero wave vector, which correspondingly determines the ordering wave vector **Q** characterizing the magnetic structure [31]. Since the Brillouin zones along the *c*-axis for the hcp and α-Sm structures are quite different, the Fermi surface for Er would also be very different for these two structures such that the nesting present along the *c*-axis in the hcp structure would not be present in the α-Sm structure and hence the disappearance of the CAM antiferromagnetic ordering [37].

IV. CONCLUSIONS

In summary, electrical resistance and X-ray diffraction measurements have been performed on erbium to temperatures down to 10 K and pressures up to 20 GPa. The Néel temperature associated with the *c*-axis modulated antiferromagnetic transition decreases with increasing pressure as determined from resistance measurements and disappears above a pressure of 10.6 GPa. The diffraction patterns also show a transition from the hcp structural phase to an α-Sm phase by 11 GPa at room temperature and between 4.6 GPa and 20.4 GPa at 10 K. These results are consistent with the CAM antiferromagnetic structure being characteristic of the hcp phase and not of the α-Sm phase under high pressure such that the disappearance of the CAM antiferromagnetic phase is the direct result of the hcp-to-Sm structural phase transition.

ACKNOWLEDGMENT

This material is based upon work supported by the Department of Energy (DOE) – National Nuclear Security Administration (NNSA) under Grant No. DE-FG52-10NA29660. Sarah A. Thomas acknowledges support from the NASA-Alabama Space Grant Consortium Graduate Fellowship program under NNX10AJ80H. Portions of this work were performed at HPCAT (Sector 16), Advanced Photon Source (APS); Argonne National Laboratory.

REFERENCES:

1. J. W. Cable, E. O. Wollan, W. C. Koehler, and M. K. Wilkinson, Phys. Rev. **140**, A1896 (1965).
2. M. Habenschuss, C. Stassis, S. K. Sinha, H. W. Deckman, and F. H. Spedding, Phys. Rev. B **10**, 1020 (1974).
3. D. Gibbs, J. Bohr, J. D. Axe, D. E. Moncton, and K. L. D'Amico, Phys. Rev. B **34**, 8182 1986).
4. H. Lin, M. F. Collins, T. M. Holden, and W. Wei, Phys. Rev. B **45**, 12 873 (1992).
5. R. A. Cowley and J. Jensen, J. Phys.: Condens. Matter **4**, 9673 (1992).
6. J. Jensen and R. A. Cowley, Europhys. Lett. **21**, 705 (1993).
7. R. V. Colvin, S. Legvold, and F. H . Spedding, Phys. Rev. **120**, 741 (1960).
8. R. W. Green, S. Legvold, and F. H. Spedding, Phys. Rev. **122**, 827 (1961).
9. B. Watson and N. Ali, J. Phys.: Condens. Matter **7**, 4713 (1995); J. Phys.: Condens. Matter **8**, 1797 (1996).
10. R. E. Skochdopole, M. Griffel, and F. H. Spedding, J. Chem. Phys. **23**, 2258 (1955).
11. H. U. Åström and G. Benediktsson, J. Phys.: Condens. Matter **1**, 4381 (1989).
12. J. J. Rhyne and S. Legvold, Phys. Rev. **140**, A2143 (1965).
13. R. S. Eccleston and S. B. Palmer, J. Phys.: Condens. Matter **4**, 10037 (1992).
14. S. W. Zochowski and K. A. McEwen, J. Mag. Mag. Mater. **140-144**, 1127 (1995).
15. S. Kawano, B. Lebech, and N. Achiwa, J. Phys.: Cond. Matter **5**, 1535 (1993).
16. S. Kawano, S. Aa. Sørensen, B. Lebech, and N. Achiwa, J. Magn. Magn. Mater. **140-144**, 763 (1995).

17. M. Ellerby, K. A. McEwen, J. Jensen, and M. J. Bull, High Pressure Research **22**, 369 (2002).

18. J. E. Milton and T. A. Scott, Phys. Rev. **160**, 387 (1967).

19. M. Ellerby, K. A. McEwen, E. Bauer, R. Hauser, and J. Jensen, Phys. Rev. B **61**, 6790 (2000).

20. D. D. Jackson, V. Malba, S. T. Weir, P. A. Baker, and Y. K. Vohra, Phys. Rev. B **71**, 184416 (2005).

21. Erbium foil, 0.1-mm thick, Johnson-Matthey product number 10170, 99.9% (REO).

22. dc magnetic susceptibility measurements were performed using a Quantum Design SQUID magnetometer model MPMS-5S.

23. S. T. Weir, J. Akella, C. A. Ruddle, Y. K. Vohra, and S. A. Catledge, Appl. Phys. Lett. **77**, 3400 (2000).

24. Y. K. Vohra and S. T. Weir in "*High Pressure Phenomenon*" Proceedings of the International School of Physics – Enrico Fermi, Course XXLVII, edited by R. J. Hemley, G.L. Chiarotti, M. Bernasconi, and L. Ulivi, IOS press, p.87 (2002).

25. G. Tsoi, A. Stemshorn, Y. K. Vohra, P. M. Wu, F. C. Hsu, Y. L. Huang, M. K. Wu, K. W. Yeh, and S. T. Weir, J. Phys.: Condens. Matter **21**, 232201 (2009).

26. F. Birch, Phys. Rev. **71**, 809 (1947).

27. N. Velisavljevic and Y. K. Vohra, High Pressure Research **24**, 295 (2004).

28. R. J. Elliott and F. A. Wedgwood, Proc. Phys. Soc. **81**, 846 (1963).

29. H. Miwa, Prog. Theor. Phys. Japan **28**, 208 (1962).

30. A. K. Mackintosh, Phys. Rev. Lett. **9**, 90 (1962).

31. J. Jensen and A. R. Mackintosh, *Rare Earth Magnetism: Structures and Excitations* (Clarendon, Oxford, 1991).

32. G. K. Samudrala, S. A. Thomas, J. M. Montgomery, and Y. K. Vohra, J. Phys.: Condens. Matter. (to be published)

33. M. Mito, K. Matsumoto, Y. Komorida, H. Deguchi, S. Takagi, T. Tajiri, T. Iwamoto, T. Kawae, M. Tokita, and K. Takeda, J. Phys. Chem. Solids **70**, 1290 (2009).

34. W. J. Carter, S. P. Marsh, J. N. Fritz, and R. G. McQueen, NBS Special Publication **326**, 147 (1971).

35. J. R. Bannister, S. Legvold, and F. H. Spedding, Phys. Rev. **94**, 1140 (1954).

36. F. J. Darnell, Phys. Rev. **132**, 1098 (1963).

37. This explanation is based on a suggestion by one of the referees.

Figure Captions:

Figure 1: The temperature dependence of the dc magnetic susceptibility on a disk-shaped sample cut from the 0.1-mm thick erbium foil. The measurements are at ambient pressure for magnetic fields applied perpendicular and parallel to the disk with the antiferromagnetic transition at 82 K being more discernible for fields applied perpendicular to the disk.

Figure 2: The four-probe electrical resistance results for erbium at various pressures for the temperature range of 10 K to 100 K and for (a) run 1 and (b) run 2. All the resistance curves have been normalized at 100 K. The antiferromagnetic transition is marked by an abrupt change in the slope of the electrical resistance with decreasing temperature.

Figure 3: Normalized resistance for various pressures after a linear temperature dependent fit ($a+bT$) to the normalized resistance for temperatures above T_N has been subtracted from the data. The inset is the experimental procedure for the determination of the antiferromagnetic Néel temperature T_N at 1.8 GPa.

Figure 4: The Néel temperature T_N as a function of pressures for the two different experimental runs. The solid curve is a linear fit to all data. The vertical dashed line indicates the pressure at which the *c*-axis modulated (CAM) antiferromagnetic ordering disappears.

Figure 5: The integrated X-ray diffraction profiles from the image plate data for erbium at (a) room temperature and (b) 10 K for different pressures. The diffraction peaks are labeled by their respective Miller indices. The peaks labeled with an asterisk are Cu peaks used for pressure determination.

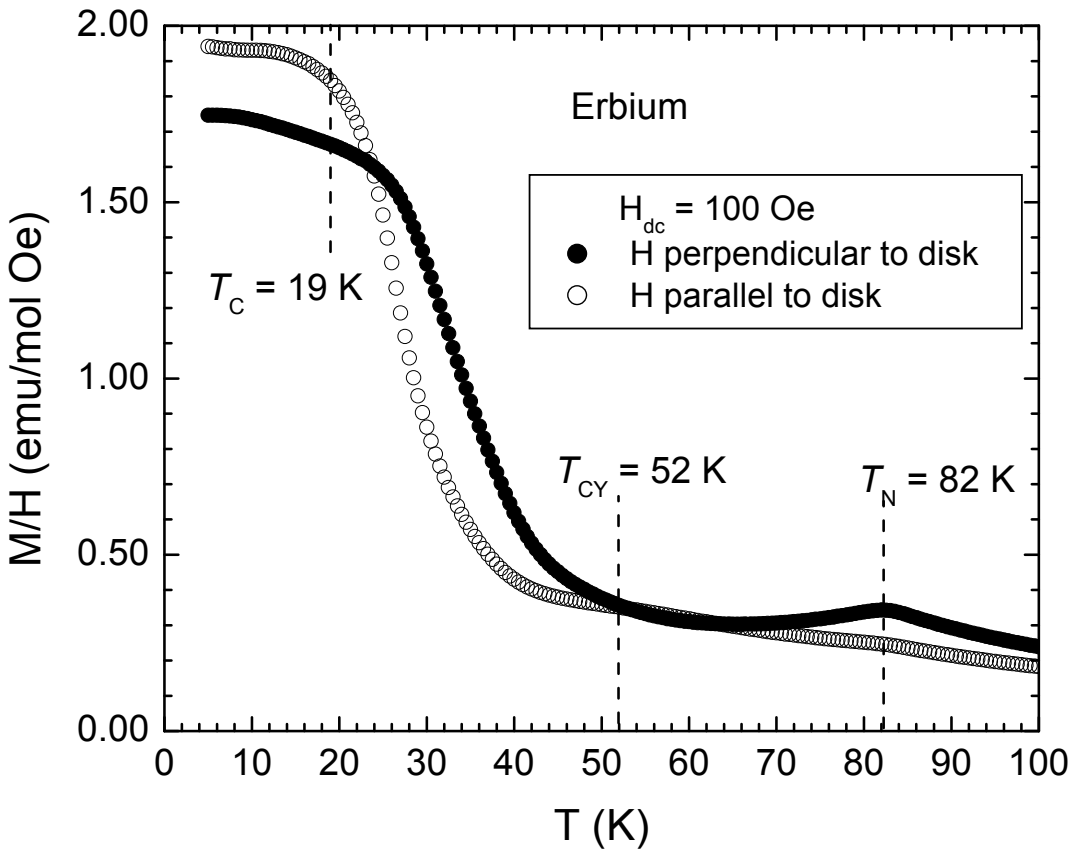
Erbium
H_{dc} = 100 Oe
H perpendicular to disk
H parallel to disk
T_C = 19 K
T_{CY} = 52 K
T_N = 82 K
M/H (emu/mol Oe)
T (K)
2.00
1.50
1.00
0.50
0.00
0
10
20
30
40
50
60
70
80
90
100

FIGURE 1

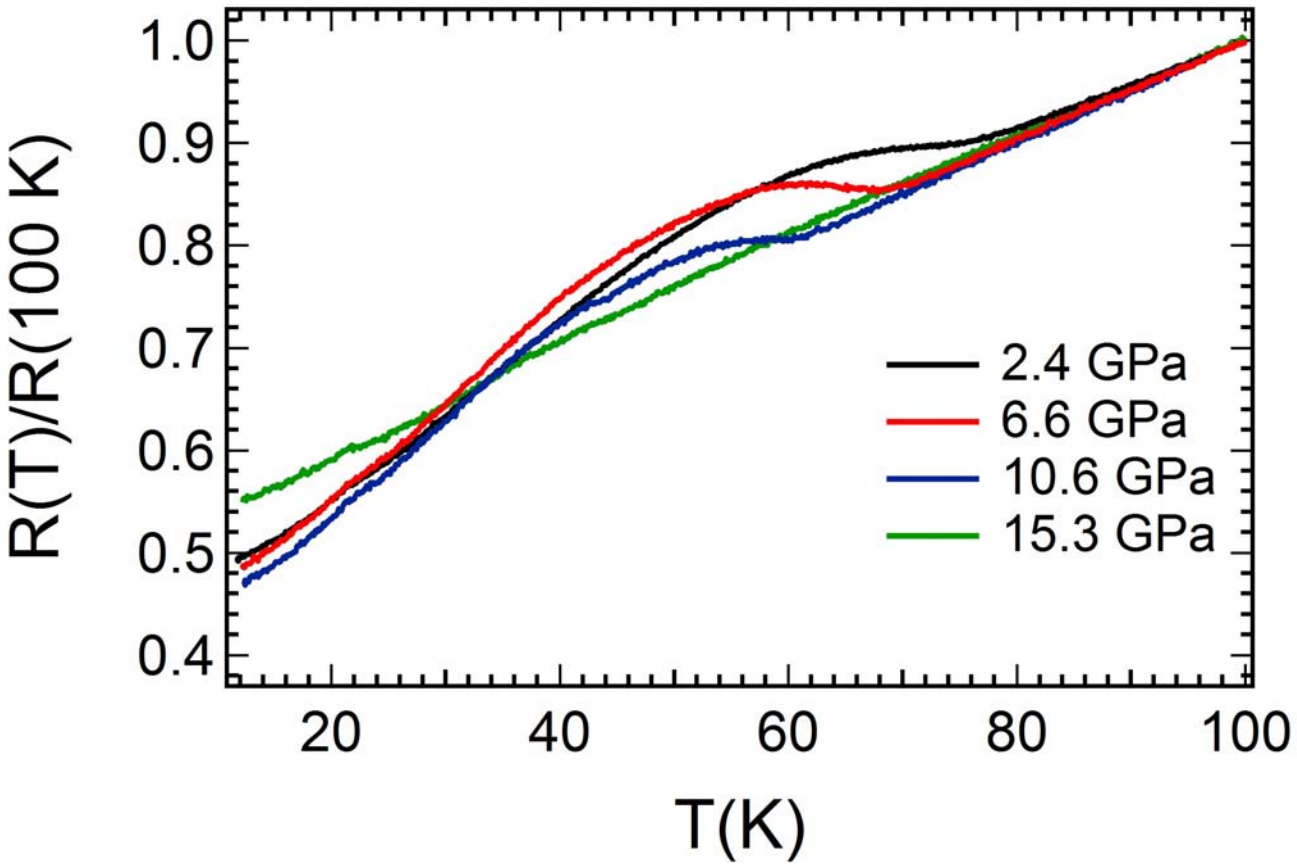
R(T)/R(100 K)
1.0
0.9
0.8
0.7
0.6
0.5
0.4
20
40
60
80
100
T(K)
2.4 GPa
6.6 GPa
10.6 GPa
15.3 GPa

FIGURE 2a

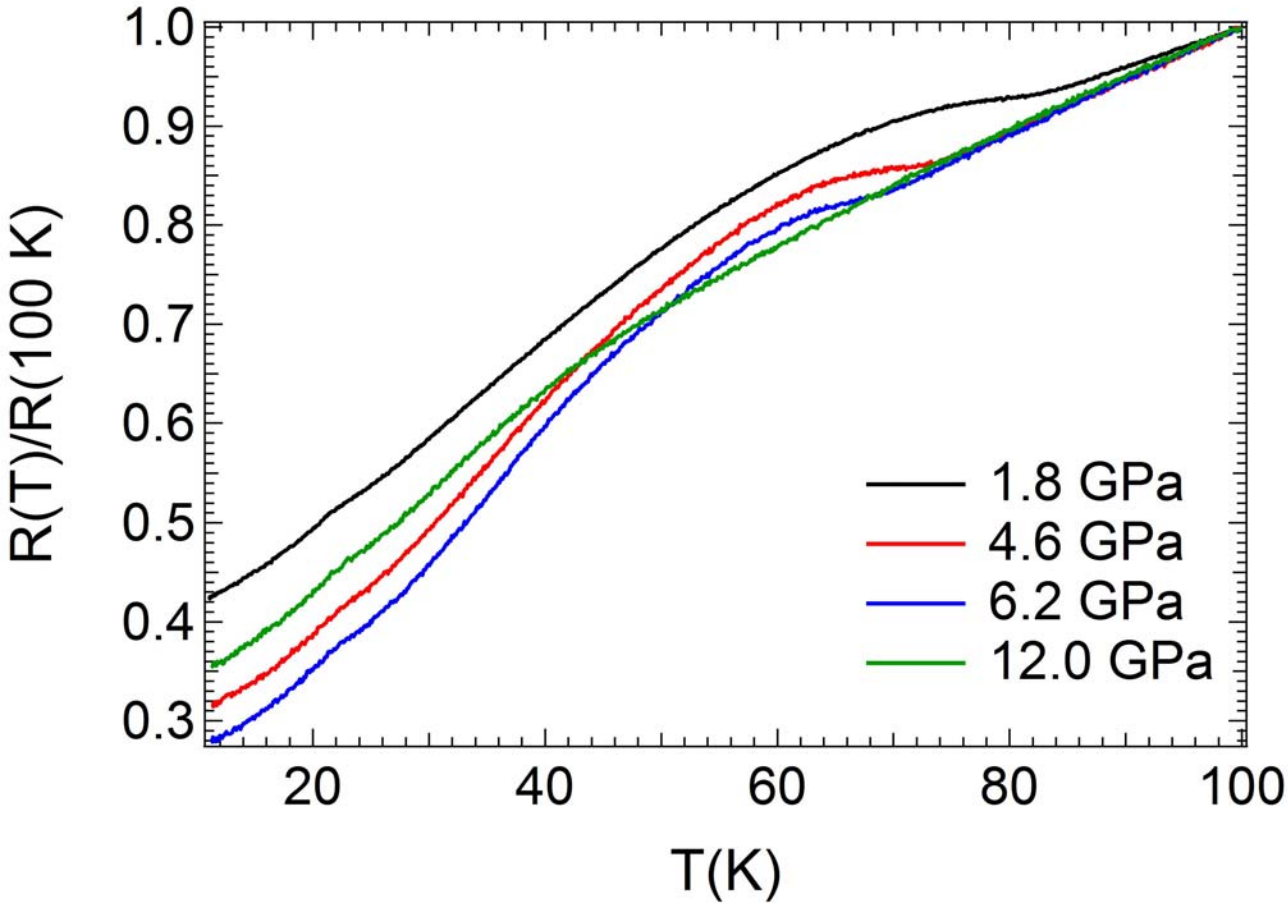
1.0
0.9
0.8
0.7
0.6
0.5
0.4
0.3
R(T)/R(100 K)
20
40
60
80
100
T(K)
1.8 GPa
4.6 GPa
6.2 GPa
12.0 GPa

FIGURE 2b

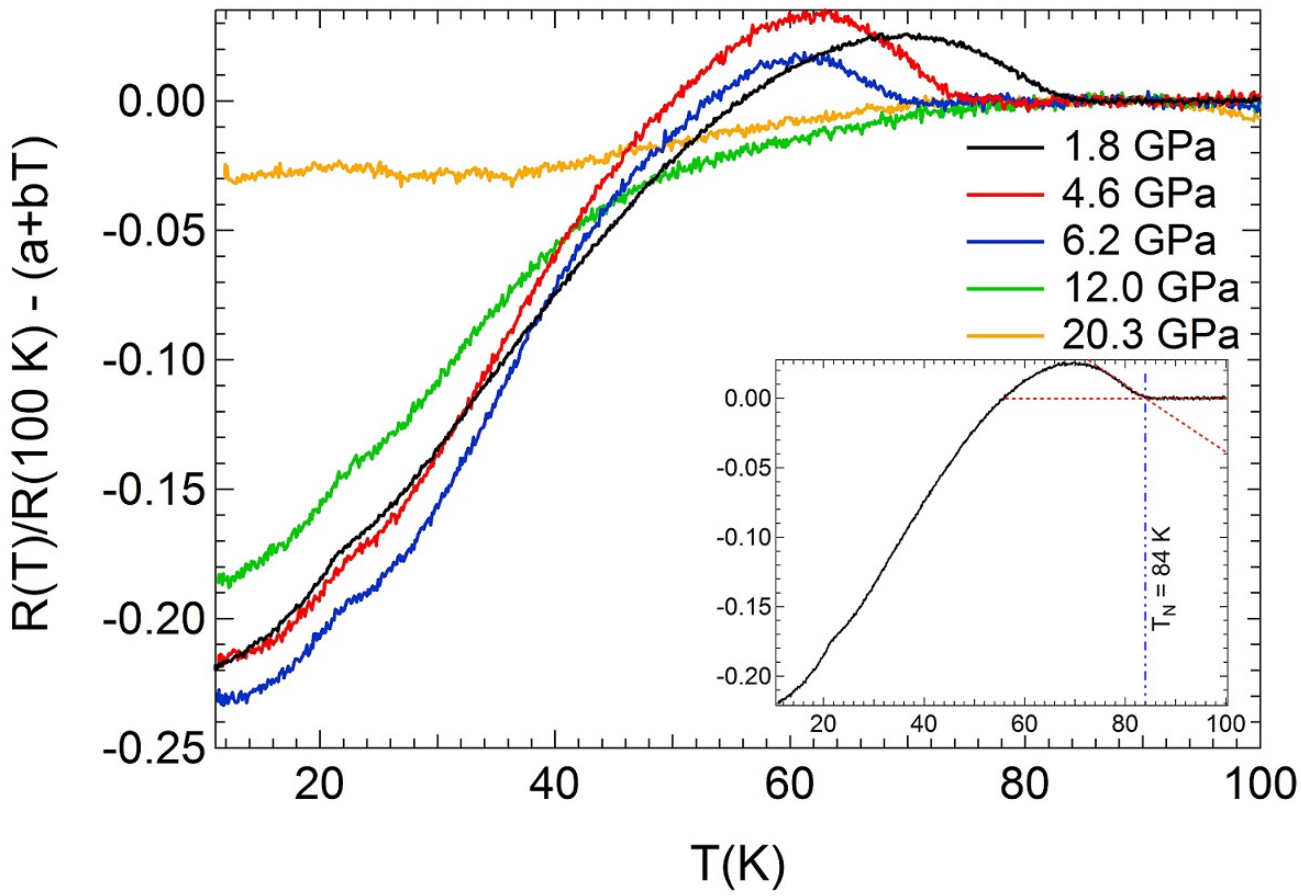
R(T)/R(100 K) - (a+bT)
T(K)
0.00
-0.05
-0.10
-0.15
-0.20
-0.25
20
40
60
80
100
1.8 GPa
4.6 GPa
6.2 GPa
12.0 GPa
20.3 GPa
T_N = 84 K

FIGURE 3

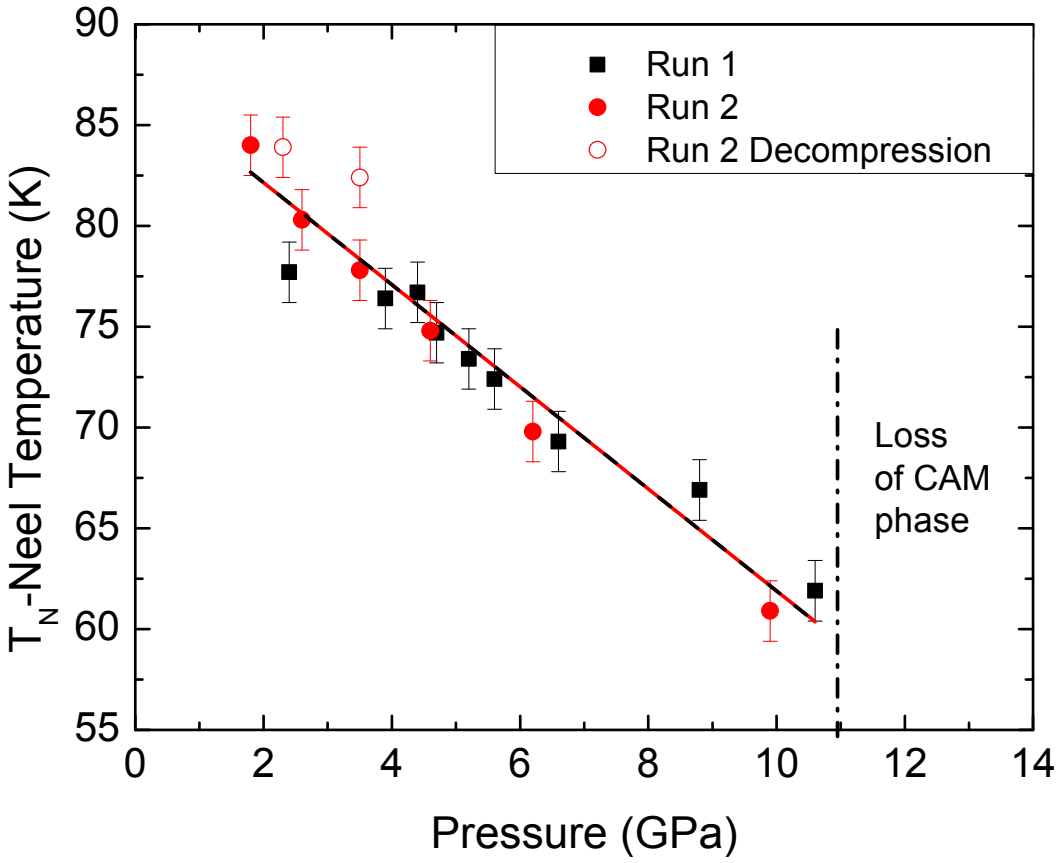
Run 1
Run 2
Run 2 Decompression
Loss
of CAM
phase
T_N-Neel Temperature (K)
Pressure (GPa)
90
85
80
75
70
65
60
55
0
2
4
6
8
10
12
14

FIGURE 4

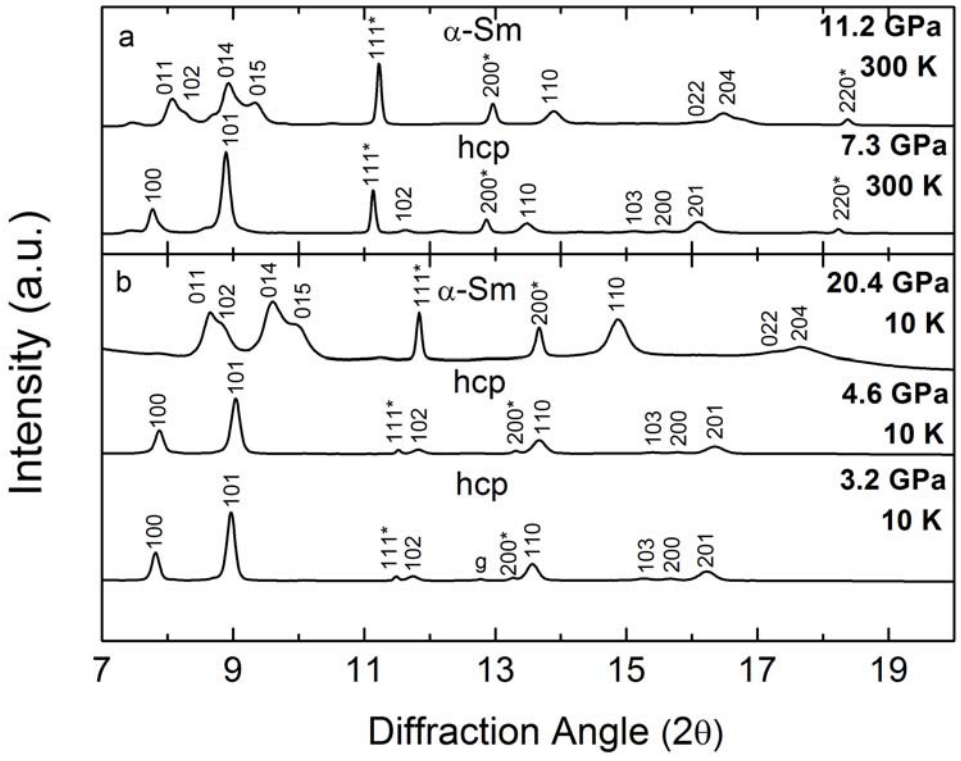
a
α-Sm
11.2 GPa
300 K
011
102
014
015
111*
200*
110
022
204
220*
hcp
7.3 GPa
300 K
100
101
111*
102
200*
110
103
200
201
220*
b
α-Sm
20.4 GPa
10 K
011
102
014
015
111*
200*
110
022
204
hcp
4.6 GPa
10 K
100
101
111*
102
200*
110
103
200
201
hcp
3.2 GPa
10 K
100
101
111*
102
200*
110
103
200
201
Intensity (a.u.)
7
9
11
13
15
17
19
Diffraction Angle (2θ)

FIGURE 5